The Opdc missense mutation of Pax2 has a milder than loss-of-function phenotype

Human Molecular Genetics, 2011, Vol. 20, No. 2 **223–234**
doi:10.1093/hmg/ddq457
Advance Access published on October 13, 2010

The *Opdc* missense mutation of *Pax2* has a milder than loss-of-function phenotype

Sally H. Cross[1,*], Lisa McKie[1], Katrine West[1], Emma L. Coghill[2], Jack Favor[3], Shoumo Bhattacharya[4], Steve D.M. Brown[2] and Ian J. Jackson[1]

[1]Medical and Developmental Genetics Section, MRC Human Genetics Unit, Institute of Genetics and Molecular Medicine, Edinburgh EH4 2XU, UK, [2]MRC Mammalian Genetics Unit, Harwell Science and Innovation Campus, Harwell OX11 ORD, UK, [3]Institute of Human Genetics, Helmholtz Zentrum München, German Research Center for Environmental Health, D-85764 Neuherberg, Germany and [4]Department of Cardiovascular Medicine, University of Oxford, Wellcome Trust Centre for Human Genetics, Oxford OX3 7BN, UK

Received August 24, 2010; Revised and Accepted October 8, 2010

Renal-coloboma syndrome, also known as papillorenal syndrome, is an autosomal dominant human disorder in which optic disc coloboma is associated with kidney abnormalities. Mutations in the paired domain transcription factor *PAX2* have been found to be the underlying cause of this disease. Disease severity varies between patients, and in some cases, renal hypoplasia has been found in the absence of any retinal defects. Here we report an *N*-ethyl-*N*-nitrosourea-induced mouse mutation, *Opdc*, which is an isoleucine to threonine missense mutation, I40T, in the first α-helix of the Pax2 paired domain. The mutant protein binds target DNA sequences less strongly than the wild-type protein and acts poorly to transactivate target promoters in culture. The phenotypic consequence of this mutation on the development of the eye and ear is similar to that reported for null alleles of *Pax2*. However, in homozygotes, cerebellar development is normal on a genetic background in which loss of *Pax2* results in failure of cerebellar formation. Moreover, there is a genetic background effect on the heterozygous phenotype such that on some strain backgrounds, kidney development is unaffected. *Opdc* is the first hypomorphic mutation reported for *Pax2* that differs in phenotype from loss-of-function mutations. These results suggest that *PAX2* is a strong candidate gene for cases in which human patients have optic disc coloboma not associated with renal dysplasia.

INTRODUCTION

Papillorenal syndrome (OMIM 120330, also known as renal-coloboma syndrome or RCS) is an autosomal dominant human disease in which abnormalities of the optic disc and retina are associated with renal malformations and vesicoureteral reflux (1). In many cases, mutations of the transcription factor *PAX2* have been found to be associated with the disease (2). The disease severity varies even within families, and in some cases, kidney defects can manifest without the associated eye disorder (3,4). In addition, hearing loss is part of the syndrome in some families (3), and there has been a rare case described in which Chiari 1 malformation of the cerebellum was found in a patient with eye and renal defects associated with a *PAX2* mutation (5). *Pax2* is a member of the PAX family of transcription factors that all contain the paired domain, a conserved 128 amino acid DNA-binding domain (6,7). This domain has a bipartite structure consisting of two structurally independent globular subdomains, each containing three α-helices connected by a linker region. Both subdomains bind to specific DNA sequence motifs in recognition sites enabling PAX2 to control the expression of target genes (8,9). The importance of the two subdomains in binding site recognition is not equivalent however; the N-terminal subdomain makes a more significant contribution to DNA binding than the C-terminal subdomain (8,10,11). Almost all of the *PAX2* mutations that have been found are predicted to be loss of function as they are termination,

*To whom correspondence should be addressed. Tel: +44 1313322471; Fax: +44 1314678456; Email: sally.cross@hgu.mrc.ac.uk

splice site mutations or insertions and deletions of variable length (reviewed in 12). Only two missense mutations have been found to be associated with RCS, both in the N-terminal subdomain of the paired domain (13,14). The G76S mutation is located immediately after the third α-helix of this subdomain and is thought to disrupt protein folding (13). Structural studies on the PAX6 paired domain show that the small side chain of the equivalent glycine residue is important to pack against the side chain of a tyrosine residue in the hydrophobic core of the N-terminal subdomain (11). The R71T mutation is found close by within the third α-helix of the N-terminal subdomain, which is the sequence recognition helix and fits into the major groove of the DNA (14). The equivalent arginine residues in the paired domains of *Drosophila* prd and human PAX6 proteins directly interact with the DNA recognition sequence (9,11). Substitution of arginine by threonine presumably disrupts target site recognition, although this has not been investigated.

Several mouse models of *PAX2* disease have been engineered or identified. Two *Pax2* mutations have been found to date by screening mice for phenotypic variation. Interestingly, the mutations are very similar to ones already described in humans and produce similar defects. The $Pax2^{1Neu}$ allele is an insertion of a single G, expanding a tract of seven Gs to eight (15). This is identical to the mutation in a severely affected patient with cerebellar, in addition to eye and kidney, defects (16). Another recently reported mutation, found by screening mutagenized mice, results in a threonine to alanine substitution at codon 74 (T74A) (17). This is the final amino acid of the third α-helix of the N-terminal subdomain of the paired domain and is equivalent to T75 in the human protein. It is located immediately before the position of the human missense mutation G76S described earlier and is part of a two-amino-acid duplication in a human patient with RCS (13). All mouse mutations, including the T74A missense mutation, have very similar heterozygous phenotypes, which model the human disorder, comprising dysplasia of the optic disc and associated retinal and vascular defects, occasional unilaterally absent kidneys and frequent small or polycystic kidneys. The mouse models allow investigation of the homozygous phenotype, which further illuminates the role of Pax2 in development. Mice homozygous for loss of the gene fail to develop kidneys, die at birth and have colobomas due to the failure of the optic fissure to close (18,19). In addition, the mutants have an absence of cochlea in the inner ear and additional brain defects (19). Genetic background modulates the effects of loss of function of *Pax2* on brain development. *Pax2* mutants on the C3H genetic background lack a cerebellum and parts of the hindbrain (15), whereas on the C57BL/6 genetic background, this defect is not seen (20). Exencephaly occurs in 100% of *Pax2*-deficient embryos on the 129SvPas (129S2) genetic background, whereas on the C57BL/6 background, the frequency drops to 30% (20). We describe here the identification of a *Pax2* mutation in the *Opdc* mutant line. The phenotype of heterozygous mice is milder than described for loss-of-function mutations. Consistent with this, the mutant protein is still able to bind to Pax2 target sequences, albeit at lower affinity, and retains the ability to stimulate transcription from some promoters. In addition, the expression levels of downstream target genes we tested are not significantly affected in heterozygotes.

RESULTS

Opdc is a point mutation in the *Pax2* gene

We identified the *N*-ethyl-*N*-nitrosourea (ENU)-induced mouse mutation, optic disc coloboma (*Opdc*), in a screen for dominant eye mutations. Mice that carry *Opdc* have bilateral colobomas of the optic disc (21). We previously mapped *Opdc* between the markers *D19Mit46* and *D19Mit103* on chromosome 19 (21). Within this interval, the paired box containing transcription factor, *Pax2*, is a strong candidate for the *Opdc* mutation because of the similarity between the retinal phenotype observed in *Opdc* heterozygotes and in mice heterozygous for known mutant alleles of *Pax2*, such as the spontaneous mutation $Pax2^{1Neu}$ (15) and the targeted alleles, for example, $Pax2^{tm1Pgr}$ (18). We amplified by polymerase chain reaction (PCR) and sequenced the exons of *Pax2* and their flanking regions from *Opdc* mutant mice, the parental strain BALB/cAnN and the two strains used to map and maintain the mutation, C3H/HeH and C57BL/6. We found a single nucleotide change, a T-to-C transition in exon 2 at position 119 (numbering from RefSeq entry NM_011037.3), in the *Opdc* allele absent from the three background strains (Fig. 1A). This causes a non-conservative missense mutation, I40T, exchanging the hydrophobic amino acid isoleucine for the nucleophilic and hydrophilic amino acid threonine. The affected isoleucine is located in the first α-helix of the N-terminal subdomain of the DNA-binding paired domain and is conserved both among other members of the PAX family of transcription factors and across species (Fig. 1B). In spite of the non-conservative nature of the amino acid substitution induced by the mutation, secondary structure prediction using the program JPRED suggests that the I40T mutation would not disrupt the helical structure of this helix (data not shown). Although I40 is in the paired domain, its position in the three-dimensional (3D) model structure suggests that it does not directly contact DNA (Fig. 1C). The structure of the paired domain of the closely related proteins PAX6 and PAX5 bound to their DNA recognition sites has been determined (11,22). The equivalent isoleucine in these structures is in the first α-helix, remote from the DNA recognition sequence and not in a position where it can directly contact DNA (Fig. 1C). Sequencing of *Pax2* reverse transcription (RT)–PCR products from *Opdc* mutant mice showed that the mutant allele is transcribed and correctly spliced (data not shown).

The heterozygous *Opdc* phenotype is milder than *Pax2* loss of function and is background-dependent

The $Pax2^{1Neu}$ loss-of-function mutation results in a significant degree of lethality of carriers (23). We initially noted that with *Opdc* after crossing to C57BL/6J for more than nine generations, only about two-thirds of the expected number of heterozygotes survived to weaning (Table 1) ($\chi^2 = 10.7$, d.f. = 1, $P < 0.01$). However, this is background strain-dependent. When we backcrossed the mutation onto a C3H background

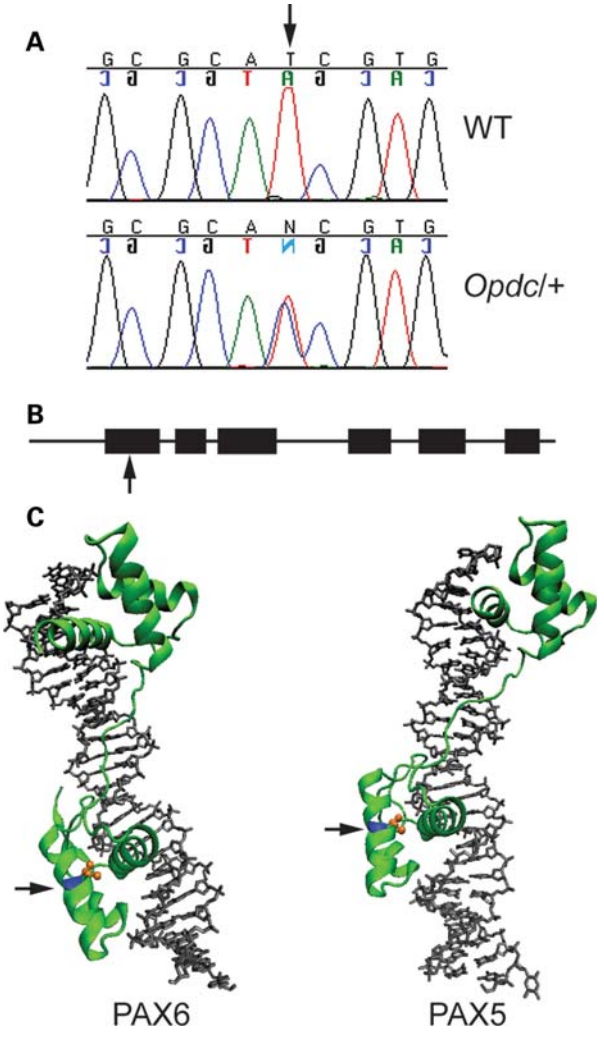

Figure 1. *Pax2* is mutated in *Opdc* mice. (**A**) Genomic DNA sequence traces from *Pax2* exon 2 from wild-type (WT) and heterozygous mutant (*Opdc*/+) mice. The arrow points to the position of the T-to-C transition. (**B**) Schematic diagram of the Pax2 paired domain. The black boxes represent the α-helices, and the arrow points to the position of the isoleucine to threonine mutation generated by the *Opdc* mutation in the first α-helix of the paired domain. (**C**) The isoleucine mutated in *Opdc* is located in the first α-helix of the paired domain and does not directly interact with the DNA-binding site. The structure of the PAX6 paired domain complexed with DNA (11) is shown on the left, and the structure of the PAX5 paired domain complexed with DNA (22) is shown on the right; crystal structures 6PAX and 1K78, respectively (http://www.pdb.org date last accessed 26/10/2010). The structures are drawn using the VMD program (55). The DNA-binding sites are shown in grey, and the paired domains are shown in green with the equivalent isoleucines to I40 in the Pax2 paired domain indicated by black arrows and coloured blue with the side chain shown in orange and drawn as scaled van der Waals spheres with cylinders as bonds. In both cases, the highlighted isoleucine is in the first α-helix positioned away from the DNA recognition site in the hydrophobic pocket with the side chain pointing towards the third α-helix where the majority of protein–DNA interactions take place.

for four or more generations, there was no detectable loss of heterozygotes ($\chi^2 = 0.26$, d.f. $= 1$, $0.9 > P > 0.5$), but note that there is a low incidence of exencephaly (discussed subsequently). The lethality on the C57BL/6J background occurs post natally, as the expected numbers of each genotype are present at embryonic stages in both strains (Table 1). The heterozygous phenotype for loss of *Pax2* function in humans or mice consistently includes severe kidney defects, which would account for the loss of carriers on some backgrounds. In mice heterozygous for a loss-of-function mutation, kidneys are ∼60% the size of wild-type, and the number of nephrons formed is significantly reduced (24,25). In addition, unilateral kidney agenesis has been reported in 4–6% of these mice (15,25). We measured kidney weight at E18.5 from heterozygous *Opdc* embryos and their wild-type littermates (Table 2). There was no significant difference in the kidney weight, corrected for total embryonic weight, between wild-type and *Opdc* heterozygous embryos on a C3H background, but on the C57BL/6J background, the heterozygous kidneys were, on average, 71.5% the size of wild-type. The reduced kidney size was also paralleled by reduced glomeruli number in mutants on this background (although statistical significance is marginal), but on a C3H background, there was no difference in the glomeruli number (Table 3). We noted unilateral renal agenesis in 1/21 heterozygous embryos on the C57BL/6J background and 0/13 on the C3H background.

Homozygous *Opdc* phenotype

Homozygotes for existing mutant alleles of *Pax2* are embryonically lethal or suffer neonatal death, probably due to kidney agenesis (15,18). *Opdc* also causes embryonic lethality when homozygous. One hundred offspring from intercrosses of $Pax2^{Opdc/+}$ animals were genotyped at weaning; no homozygotes were detected, whereas 61 were heterozygous and 39 wild-type. To ascertain the causes of lethality and to examine any other phenotypic effects of the *Opdc* mutation, embryos derived from $Pax2^{Opdc/+}$ intercrosses were recovered at various development stages and used for morphological and histological analyses. We find the homozygous phenotypes of the kidney, ear and eye to be very similar to those described for existing loss-of-function mutations (15,18,19). Magnetic resonance imaging (MRI) scans of homozygous embryos at E15.5 indicated that the kidneys were absent (Fig. 2E–G, compare with MRI scans from E15.5 heterozygous embryos in Fig. 2I–K). From the MRI scans, the eye appears malformed in the homozygous mutant (Fig. 2H, compare with wild-type and heterozygous in Fig. 2D and L). Histological sections through the eyes of E15.5 homozygotes and heterozygotes showed expansion of the retina down the optic stalk in both, as described previously for *Pax2* null mutants, and the abnormal phenotype was more severe in homozygotes than in heterozygotes (3B) (15,19). Scans of the inner ear revealed severe abnormalities; after 3D rendering, the semi-circular canals appear grossly dilated and the cochlea is malformed (Fig. 3A). Similar abnormalities have been reported for loss-of-function alleles of *Pax2* (19).

Pax2 is involved in the specification of the midbrain–hindbrain boundary and in neural tube closure, although the severity of the phenotype is affected by the genetic background (15,20). To assess the effect of the *Opdc* mutation on different genetic backgrounds, we crossed it onto C57BL/6J or onto C3H for at least four generations and intercrossed $Pax2^{Opdc/+}$ mice to generate homozygous mutant embryos and wild-type littermates at E15.5. We find that *Opdc*

Table 1. Mice or embryos wild-type, homozygous or heterozygous for the *Opdc* mutation on two genetic backgrounds

Background strain	Stage	Cross	++	$Pax2^{Opdc/+}$	$Pax2^{Opdc/Opdc}$	*P*-value[a]
C57BL/6J	Weaning	$Pax2^{Opdc/+}$ × wild-type	137	88	N/A	<0.01
C3H	Weaning	$Pax2^{Opdc/+}$ × wild-type	131	123	N/A	>0.5
C57BL/6J	Embryo, E15.5 to E18.5	$Pax2^{Opdc/+}$ × $Pax2^{Opdc/+}$	30	63	26	>0.5
C3H	Embryo, E15.5 to E17.5	$Pax2^{Opdc/+}$ × $Pax2^{Opdc/+}$	32	49	28	>0.1

[a]Test for significance using χ^2 test.

homozygote embryos have exencephaly with variable penetrance, depending on the genetic background. On the C57BL/6J background, 30% (6/20) of the homozygous mutant embryos showed the phenotype, whereas on the C3H background, the penetrance increased greatly to 95% (20/21). There is also a low level of exencephaly seen in heterozygotes, about 2% (1/47) on the C57BL/6J background and 12% (4/34) on the C3H background. The hindbrain developmental phenotype of homozygous *Pax2* loss-of-function mutants also varies according to the genetic background. On a largely C3H background, homozygotes fail to form a cerebellum (15). In contrast, cerebellar formation is normal on the C57BL/6J background (20). In contrast to null alleles of *Pax2*, we found that the cerebellum was present in *Opdc* homozygotes regardless of the genetic background (Fig. 3C).

In conclusion, aspects of the *Opdc* heterozygous and homozygous phenotypes are less severe than those reported for loss-of-function alleles, which suggests that the mutant Opdc Pax2 protein retains some function and that the allele is a hypomorph.

DNA-binding properties of $Pax2^{Opdc}$

Structural predictions suggest that the mutant amino acid found in the Opdc Pax2 paired domain is not involved in direct DNA contact (Fig. 1C). However, it is possible that the mutation perturbs the structure of the paired domain. Therefore, we investigated the effect of the mutation on the binding of the Pax2 paired domain to target DNA sequences. We produced and purified recombinant His-tagged paired domains from wild-type and Opdc mutant Pax2 proteins and used these in bandshift experiments with a number of known Pax2 binding sites (Fig. 4E). First, we used the high affinity Pax2 binding site, Pax2Con (26), as a probe. Both wild-type and *Opdc* paired domains formed a complex with Pax2Con that resulted in a robust gel shift (Fig. 4A). However, when we used the suboptimal site e5, which is a target site of the *Drosophila prd* gene (27), as a probe, the Opdc Pax2 paired domain did not form a complex, although the wild-type Pax2 paired domain did (Fig. 4A). This suggested that the *Opdc* mutation prevents the binding of the Pax2 paired domain to suboptimal target sites. To compare the strength of the binding of the wild-type and mutant Pax2 paired domains to an optimal binding site, we performed a competition bandshift using labelled Pax2Con as a probe and adding increasing amounts of unlabelled Pax2Con as competitor (Fig. 4B). The Opdc paired domain complex was disrupted at lower concentrations of the Pax2Con competitor compared with the wild-type complex, indicating that the mutant protein was bound less tightly than the wild-type (Fig. 4B). When unlabelled e5 probe was used as competitor, neither the wild-type nor the mutant Pax2Con–protein complexes were disrupted (data not shown). Thus, although the *Opdc* mutation does not abolish the ability of its paired domain to bind to the strong binding site (Pax2Con), it does reduce the affinity of the interaction. With less favourable binding sequences such as e5, the *Opdc* mutation prevents binding of the paired domain. Although these results suggest that *Opdc* is a hypomorphic mutation, neither of these sequences have been described in bona fide *in vivo* Pax2 binding sites. To assess the effect on the interaction of the Pax2 paired domain with authentic binding sites, we used binding sites as probes that have been found in the upstream region of Pax6 (P6), the upstream region of Pax2 (P2) and in Pax6 retinal enhancer (Enh) (28) (Fig. 4E). The wild-type Pax2 paired domain bound to all as expected (Fig. 4C). In contrast, the Opdc paired domain bound to P2, bound weakly to P6 but could not bind to Enh (Fig. 4C). We also tested sites Dd and Pc that have been identified upstream of the *Pou3f3* gene (Fig. 4E) (29). In this case, the Opdc paired domain could bind to the Dd site, albeit less strongly than wild-type and bound only weakly to the Pc site (Fig. 4D). These results demonstrate differential binding of the wild-type and mutant paired domains to mouse Pax2 targets. Although the Opdc mutant protein is able to bind to most target DNA sites, the affinity of binding is variable and reduced at some of the binding sites. There appears to be a correlation between the capability of the *Opdc* paired domain to bind and the similarity of the site to the consensus (Fig. 4E). The e5 and Enh sites that were not bound by the Opdc paired domain match least well to the Pax2 consensus binding sequence.

Transcriptional activation by Opdc mutant Pax2

We next investigated the ability of wild-type and mutant Pax2 protein to transactivate transcription in a reporter assay. There are two major isoforms of the Pax2 protein, which include or omit 23 amino acids encoded by the alternatively spliced exon 6 (30); these are the long and short isoforms Pax2a and Pax2b designated P32114-1 and P32114-2, respectively (http://www.uniprot.org date last accessed 26/10/2010). We introduced the *Opdc* mutation into constructs expressing each form, CMV-Pax2a and CMV-Pax2b (31). We tested the ability of these to transactivate a luciferase reporter gene downstream of various Pax2 binding sites by transiently co-transfecting constructs into NIH-3T3 cells (Fig. 5). We examined the effect of each wild-type and mutant isoform of the Pax2 protein on a promoter containing five tandem copies of the

Table 2. Kidney mass as fraction of total embryo mass of E18.5 embryos wild-type or heterozygous for the *Opdc* mutation, in two strains

Background strain	Genotype	Left kidney, % of total embryo mass (*N*)	Right kidney, % of total embryo mass (*N*)	Significance left versus right[a]
C57BL/6J	Wild-type	0.57 (15)	0.52 (15)	$P = 0.203$
C57BL/6J	Heterozygous	0.39 (21)	0.38 (21)	$P = 0.817$
Significance wild-type versus heterozygous[a]		$P = 0.000337$	$P = 0.007908$	
C3H	Wild-type	0.42 (11)	0.40 (11)	$P = 0.790$
C3H	Heterozygous	0.42 (10)	0.35 (10)	$P = 0.097$
Significance wild-type versus heterozygous[a]		$P = 0.970894$	$P = 0.381662$	

[a]Test for significance using *t*-test.

artificial Pax2 binding site PRS4 (32) cloned upstream of luciferase. Both wild-type proteins strongly activate the luciferase reporter gene driven by this promoter by 27- and 33-fold, which is significantly higher when the mutant versions of the protein were used (Fig. 5A). However, both Opdc mutant proteins do demonstrate weaker but significant transactivation activity on this promoter, 2.5-fold in the case of Pax2-a^{Opdc} (*t*-test, $P = 0.023$) and 7.8-fold in the case of Pax2b^{Opdc} (*t*-test, $P = 0.0013$) (Fig. 5A). In contrast, when we used two alternative promoters in this assay derived from the putative *in vivo* Pax2 targets, *Pou3f3* (29) and *RET* (25), we find that the wild-type proteins activate them much less strongly (*Pou3f3* 2.6- and 3.2-fold and *RET* 2.1- and 3.5-fold) and that the *Opdc* mutant proteins show no significant activation (Fig. 5B and C).

Transcription of downstream genes in *Pax2*$^{Opdc/+}$ mutants

To test the effect of the *Opdc* mutation *in vivo*, we examined the levels of two Pax2 target genes in *Pax2*$^{Opdc/+}$ mutant embryonic kidneys. It has been reported that the transcription of *Ret* is reduced in heterozygous *Pax2* null kidneys at E18.5 by 47.5-fold relative to the expression in wild-type kidneys (25). The genes *Wt1* and *Pax2* are thought to regulate each other's expression during kidney development, and in *Pax2*$^{1Neu/+}$ kidneys at E19, the expression of *Wt1* was reported to be elevated by 35% relative to its expression level in wild-type kidneys (23). To determine the level of expression of *Ret* and *Wt1* in *Opdc* heterozygous mice, we performed real-time quantitative RT–PCR analysis using RNA isolated from E18.5 wild-type and heterozygous *Opdc* mutant kidneys on both C3H and C57BL/6 backgrounds. To compare with the previously reported loss-of-function mutation, we assayed in parallel the level of *Wt1* and *Ret* mRNA in heterozygous *Pax2*^{1Neu} mutant kidneys on the C57BL/6 background. In contrast to previous reports, we detected no significant change in the level of expression of either gene in mice heterozygous for either mutant on either genetic background, although there was some degree of variation between individual animals of the same genotype (Fig. 6).

DISCUSSION

The phenotype of mice homozygous and heterozygous for *Opdc* is similar to that of loss of function of *Pax2*, but some aspects are milder and more sensitive to genetic background. There are striking differences in the phenotypic consequences of the *Opdc* mutation on the C57BL/6J and C3H genetic backgrounds. In homozygous mutant embryos, although cerebellar development is normal on both genetic backgrounds (Fig. 3C), we observe a high incidence of exencephaly on the C3H background. On the C57BL/6J background, the viability of heterozygotes is impaired whereas on the C3H background, we observe the expected number of heterozygous mice at weaning. A similar effect on viability is seen with *Krd*/+ mice, which carry a 7-cM deletion that includes the *Pax2* gene, although the detrimental effect of the C57BL/6 background is more severe because after backcrossing *Krd* onto C57BL/6 for six generations, no *Krd*/+ offspring were found (33). This probably reflects both the impact of the C57BL/6 genetic background on viability caused by loss of one copy of *Pax2* and adverse effects on viability due to haploinsufficiency for the other genes in the deletion interval.

The mutant Pax2 protein is still able to bind to target DNA sequences, albeit with reduced affinity, and is still able to transactivate reporter genes, also with reduced efficiency. I40, the amino acid altered by the *Opdc* mutation, is located in the core of the hydrophobic pocket of the N-terminal subdomain of the paired domain with the side chain of the isoleucine (shown in orange in Fig. 1C), extending towards the third α-helix which fits into the major groove and contacts the DNA (9,11). Replacement of the hydrophobic isoleucine with the polar threonine might pull the third α-helix out of the major groove and destabilize DNA-protein binding. However, as the two subdomains do not interact and are structurally independent (8–10), the *Opdc* mutation would not be expected to affect interactions between the C-terminal subdomain and DNA, and this is what may be mediating the DNA-binding activity of the *Opdc* mutant protein. Indeed, there are alternative splice forms of Pax6 and Pax8, in which the N-terminal subdomain is disrupted, which can bind DNA recognition sequences solely via the C-terminal subdomain (10,34). We suggest that the mutant Opdc protein retains some normal Pax2 function, hence the milder phenotype, and that this residual function renders the activity of the protein more labile and more susceptible to the effects of genetic background.

Although haploinsufficiency for the related gene *PAX6* usually causes aniridia in humans (35), missense mutations in the paired domain have been found to result in variant

Table 3. Glomeruli counts in wild-type and heterozygous mice in C57BL/6J (at E18.5) and in C3H (at P0)

Background strain	Genotype	Average glomerulus count	Significance[a]
C57BL/6J	WT	13.33	
C57BL/6J	WT	11	
C57BL/6J	WT	11.66	
C57BL/6J	Het	10.66	
C57BL/6J	Het	9	
C57BL/6J	Het	8.33	$P = 0.065$
C3H	WT	17	
C3H	WT	12.5	
C3H	WT	21.5	
C3H	WT	19.5	
C3H	Het	15	
C3H	Het	13.5	
C3H	Het	21	$P = 0.4$

Glomerular density analysis on haematoxylin- and eosin-stained sections was carried out essentially as described (25).
[a]Significance assessed by *t*-test on total data.

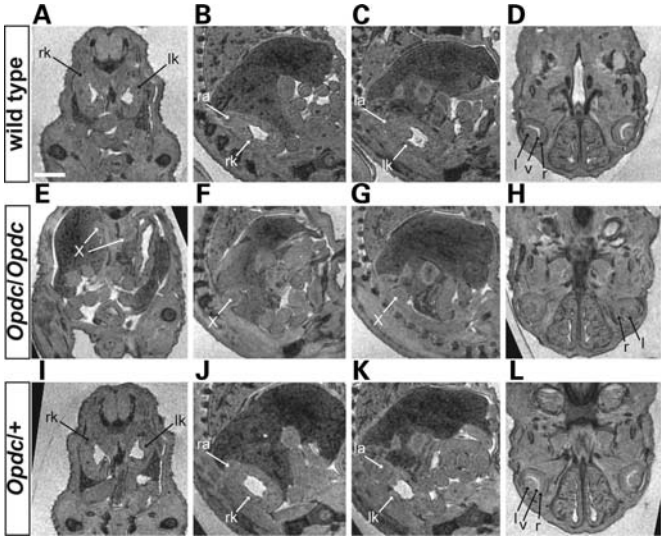

Figure 2. *Opdc* causes renal agenesis and developmental retardation of eyes. MRI of the kidneys and eyes of E15.5 embryos. (**A**–**C**) Transverse and sagittal sections showing the left and right kidneys (lk and rk) and left and right adrenals (la and ra) in a wild-type embryo. (**D**) Transverse section showing the eye structures including lens (l), vitreous (v) and retina (r) in a wild-type embryo. (**E**–**H**) Corresponding sections through a $Pax2^{Opdc/Opdc}$ embryo, showing that the kidneys are absent. The bilateral structure 'X' may be an adrenal. The eyes are poorly developed, with the vitreous not clearly seen in any section. (**I**–**L**) Corresponding sections through a $Pax2^{Opdc/+}$ embryo which looks normal. Scale bar = 50 U (1250 μm).

phenotypes. The R26G mutation underlies Peters' anomaly, a milder anterior segment eye defect than aniridia, probably because the mutant protein can bind to a subset of target PAX6 binding sites (36,37). Ectopia pupillae, congenital nystagmus and mild aniridia have been reported to be caused by missense mutations in the *PAX6* paired domain (38,39). Like *Opdc*, two of the missense mutations causing mild aniridia are located in the hydrophobic core of the N-terminal subdomain (39). Although missense mutations affecting the equivalent isoleucine in PAX6 to I40 in Pax2 have been found in two human aniridia patients, one being a change to valine and the other to serine (http://lsdb.hgu.mrc.ac.uk/home.php?select_db=PAX6 date last accessed 26/10/2010), in both cases the severity of the disease is not clear (40, G. Wildhardt, unpublished data).

There are undoubtedly genetic background effects on *PAX2* mutations in humans. Studies on patients indicate that the same mutation in *PAX2* can result in variable disease, ranging from severe eye, kidney and cerebellar defects to kidney disease with no major effect on the eye (2,3,41). Within one family with a frame-shift mutation in *PAX2*, the kidney defects were more variable than the eye abnormalities in affected individuals (2). In patients with the G76S mutation, it was noted that the eye phenotype was mild (13) and a case of isolated renal hypoplasia in a patient with a nonsense mutation in *Pax2* has been reported (42). Interestingly, in a family segregating dominantly inherited renal hypoplasia with no ocular abnormalities, a missense mutation, A111T, located in the C-terminal subdomain of the PAX2 paired domain was identified as being causative of the disease (43). Again, the severity of the disease varied greatly between individuals, ranging from bilateral renal agenesis to no apparent disease in obligate carriers.

Mouse inbred strains allow genetic background effects to be investigated more rigorously than in human patients. We have found that the dominant, partially penetrant, lethality of the $Pax2^{Opdc}$ mutation seen on C57BL/6J is largely suppressed on the C3H background. All other analyses of mouse *Pax2* mutations have found a degree of dominant lethality; we suggest that the hypomorphic nature of *Opdc* means that on certain backgrounds, the dominant kidney defect is suppressed. It will be interesting to identify the genes responsible for this suppression. Increased apoptosis during foetal kidney development has been found in heterozygous mutants (24), suggesting that strain differences in genes which trigger or are involved in this pathway might be responsible for the phenotypic differences we have observed. There are numerous examples of mouse strain-specific phenotypic modifiers, for example, dominant lethality due to loss of function of *Nkx2.5* (44), the severity of various recessive models of polycystic kidney disease (45) or the presence of cataracts in mice mutant for the vacuolated lens mutation of *Gpr161* (46). Relatively few of these modifiers of mutant phenotypes (as opposed to quantitative trait loci affecting complex genetic traits) have been mapped, and fewer still have been associated with identified genes. Matteson *et al.* (46) identified *Foxe3*, which itself results in cataracts when mutant, as the gene whose strain variation modifies the penetrance of the vacuolar cataract phenotype of *Gpr161*.

Genetic and genomic resources currently under development will greatly facilitate future identification of genetic modifiers. The collaborative cross recombinant inbred strains (47) will enable modifiers of dominant phenotypes to be relatively easily fine mapped. Furthermore, the genome sequences of many of the commonly used inbred mouse strains, including the eight used in the collaborative cross, are now available, which should allow rapid candidate gene identification (http://www.sanger.ac.uk/resources/mouse/genomes/ date last accessed 26/10/2010).

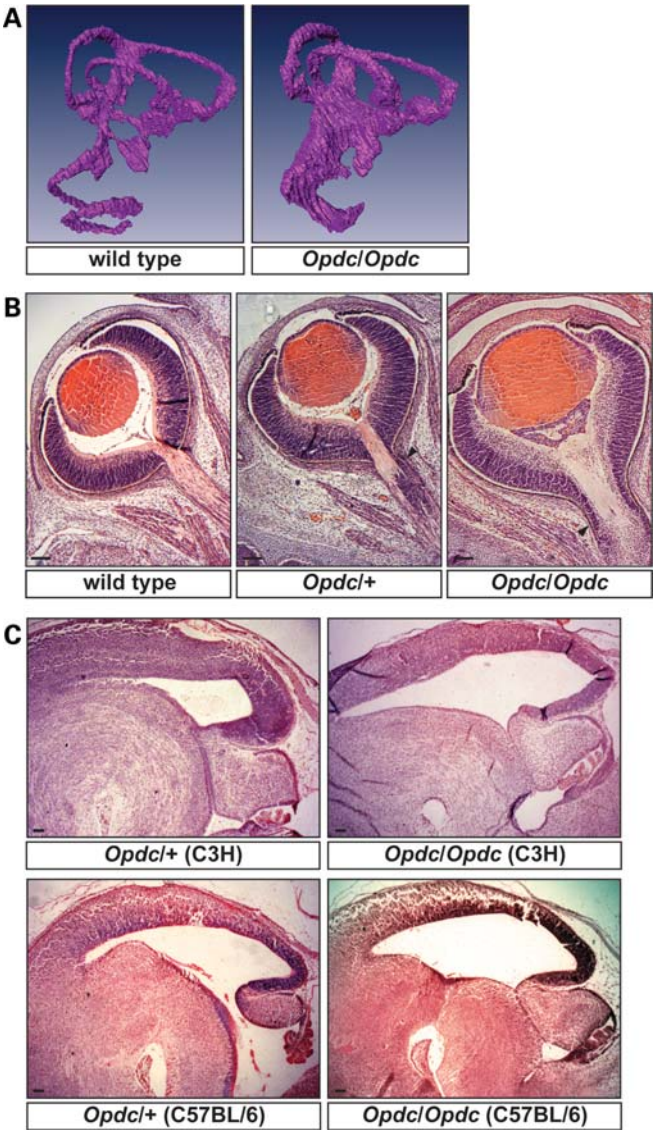

Figure 3. *Opdc* causes inner ear and eye defects but does not affect cerebellar development. (**A**) The images show the endolymphatic-filled membranous labyrinth within the cochlea and semi-circular canals from wild-type and homozygous *Opdc* mutants. The cochlea of the homozygous *Opdc* mutant is highly malformed having a broad hook shape, whereas the semi-circular canals appear comparatively normal in shape compared with that of the wild-type. (**B**) Transverse sections through embryonic eyes at E15.5. In $Pax2^{Opdc/+}$, the retina extends down the optic stalk and this is more pronounced in the $Pax2^{Opdc/Opdc}$ embryo (arrowheads). (**C**) The *Opdc* mutation does not affect cerebellar development. Transverse sections through the cerebellum at E15.5. On both the C3H and the C57BL/6 backgrounds, the cerebellum develops normally, compare $Pax2^{Opdc/Opdc}$ and $Pax2^{Opdc/+}$ embryos. Scale bar = 100 μm.

Finally, our finding that on some inbred genetic backgrounds $Pax2^{Opdc}$ heterozygotes have coloboma defect but no apparent kidney disease suggests that *PAX2* could be a candidate in human patients for colobomatous defects alone. A relatively small number of patients with isolated optic nerve coloboma or with other eye defects have been reportedly screened for mutations in *PAX2* without success (48), but a larger screen may be merited.

MATERIALS AND METHODS

Animals

The animal studies described in this paper were carried out under the guidance issued by the Medical Research Council in Responsibility in the Use of Animals for Medical Research (July 1993) and Home Office Project Licence nos PPL60/2242, PPL60/3124 and PPL60/3785. The *Opdc* strain has been submitted to the European Mouse Mutant Archive (http://www.emmanet.org/ date last accessed 26/10/2010) strain number EM:01942.

Linkage analysis

PCR products containing informative single nucleotide polymorphisms were amplified from genomic DNA extracted using standard procedures from BALB/c (the ENU-mutagenized strain), C57BL/6J (the strain used for backcrossing) and backcross progeny and sequenced as described below.

Mutational analysis of *Pax2*

The exons and the immediate flanking sequences of *Pax2* were amplified from *Opdc*, BALB/c, C3H and C57BL/6J genomic DNA using intronic primers that were also used for subsequent sequence analysis. PCR products were purified using a Millipore Multi-screen PCR 96-well filtration system on a Biomek 2000 robotic platform and sequenced directly using Big Dye™ terminator cycle sequencing. Sequences were analysed using the Sequencher™ program.

Transcription reporter assays

Transfections were carried out using a MicroPorator MP-100, following the manufacturer's protocol (Labtech International, Ringmer, East Sussex, UK). To correct for transfection efficiency and viability, 2.5 ng of renilla reporter vector was also transfected. The day following transfection, luciferase assays were carried out using the Dual-luciferase reporter assay system (E1910, Promega UK, Southampton, Hampshire, UK), and readings were normalized using the renilla reporter. Each experiment was carried out in triplicate.

Constructs and recombinant protein production

The Opdc mutation was introduced into CMV-Pax2a and CMV-Pax2b [(31), a gift of G. Dressler] by replacing the *Fse*I to *Nhe*I fragment containing the site of the *Opdc* mutation with the equivalent fragment from pHCMV-Pax2 [(49), a gift of P. Gruss] that had the *Opdc* mutation introduced into it using the QuikChange Site-Directed Mutagenesis Kit (Stratagene, Agilent Technologies, Inc., Santa Clara, CA). To make the plasmid PRS4Luc, the PRS4 binding site was amplified from pRS4CAT [(32), a gift of G. Dressler] using oligonucleotides 5′-GTTTTCCCAGTCACGACGTT-3′ and 5′-GGCCTG CAGTGCTCTGCCTTTTATGCCCAAGCTAGAGTCGAGA TATCTAGAGC-3′ and cloned into pGEMTEasy (Promega). The resulting plasmid was digested with *Sal*I and *Pst*I and the fragment containing PRS4 isolated and cloned into the *Sal*I and *Pst*I sites of Pax6enh/Luc-S [modification of

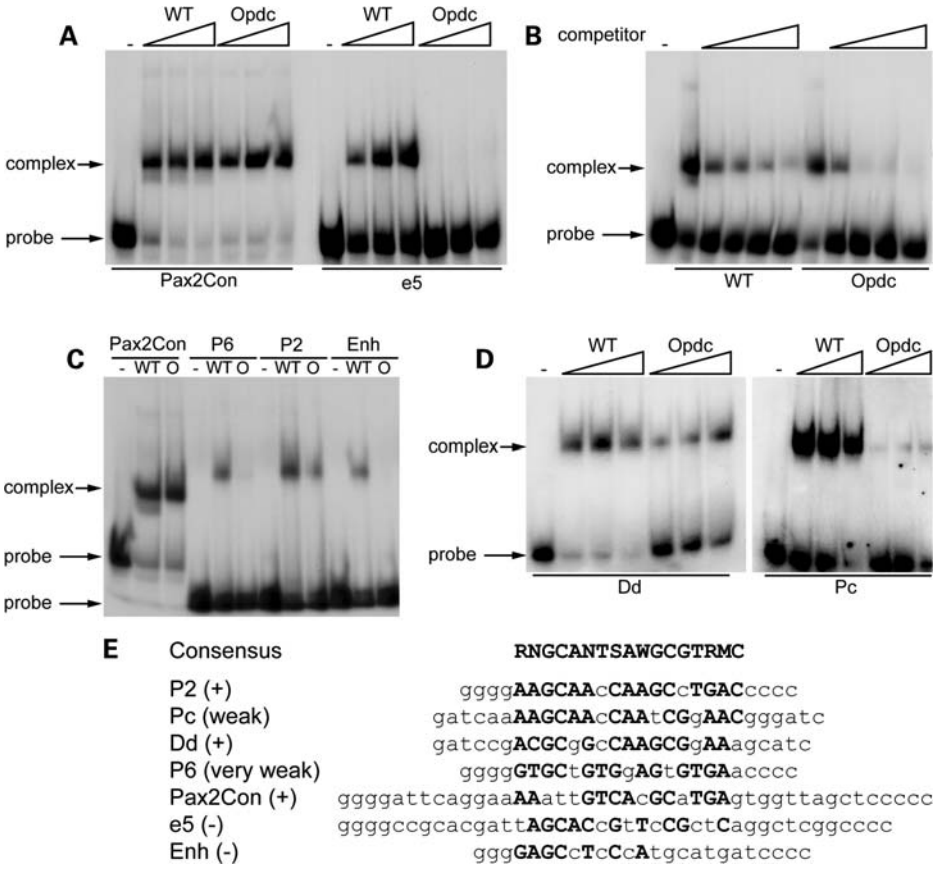

Figure 4. The Opdc mutation impairs the binding of the Pax2 paired domain to target sites. (**A**) Bandshift analysis using either the consensus Pax2 binding site Pax2Con (26) (left panel) or a less favourable probe e5 (27) (right panel) with no protein (−), increasing amounts of recombinant Pax2 paired domain with either wild-type (WT) or the *Opdc* mutation (Opdc) as indicated by the triangle. Both WT and Opdc paired domains could bind to Pax2Con, but only the WT bound to e5. (**B**) Bandshift analysis using the high affinity probe Pax2Con. In the first lane, no protein was added (−); in lanes 2–6, recombinant WT Pax2 paired domain was added and in lanes 7–11, recombinant Opdc Pax2 paired domain (Opdc) was added. Increasing amounts of unlabelled Pax2Con were added as competitor as indicated by the triangle in lanes 3–6 and lanes 8–11. The DNA–Opdc protein complex was disrupted more easily than the DNA–WT protein complex. (**C**) Bandshift analysis using Pax2Con (26), Pax2 binding sites from the *Pax2* gene promoter, P6 and P2, and a Pax2 binding site from the *Pax6* retinal enhancer region, Enh (28). Reactions with no protein (−), WT Pax2 paired domain or Opdc Pax2 paired domain (O) are shown. The WT Pax2 paired domain bound to all sites, whereas the Opdc Pax2 paired domain bound to the P2 binding site, bound very weakly to the P6 binding site and did not bind to the Enh binding site. (**D**) Bandshift analysis using either the Dd binding site (left panel) or the Pc binding site (right panel) from the *Pou3f3* gene promoter (29) with increasing amounts of recombinant Pax2 paired domain either WT or containing the Opdc mutation (Opdc) as indicated by the triangle. In the first lane of each panel no protein was added (−). The WT Pax2 paired domain bound to both sites, and although Opdc Pax2 paired domain could bind to both binding sites, it bound slightly less well than the WT to Dd and only weakly to Pc. (**E**) Sequences of the DNA probes used. At the top is the Pax2 consensus binding sequence (50), alternative nucleotides are given in positions in which the occurrence of the minor nucleotide is greater than 30%. Below this, the binding sequences used are in order of agreement with the consensus sequence. In each binding site, uppercase indicates nucleotides that are found in the consensus sequence and the degree of binding of each to the Opdc paired domain is in parentheses, + indicating good binding. The e5 and Enh probes that did not bind to the Opdc paired domain conform least well to the consensus sequence. R = A or G, N = A, G, C or T, S = G or C, W = A or T, K = T or G and M = C or A.

plasmid pluc-S (50, a gift of D.J. Kleinjan)] with the result that PRS4 is placed upstream of a luciferase reporter. To make the Pou3f3prom reporter plasmid, the following oligonucleotides, 5′-GATCTGAATTCGATCGGGCCCA-3′ and 5′-AGCTTGG GCCCGATCGAATTCA-3′, were annealed and cloned into the *Bgl*II and *Hin*dIII sites of the pGL3-Basic vector polylinker (Promega) to introduce *Eco*RI and *Psp*OMI restriction sites and to create vector pGL3-BasicLink. The 3.2 kb *Bgl*II–*Not*I fragment of the Pou3f3 gene promoter from bacterial artificial chromosome clone RP23-347M3 that contains the Dd and Pc binding sites was cloned into the *Bgl*II and *Psp*OM1 sites of pGL3-BasicLink to make Pou3f3prom. All constructs were verified by sequencing.

To produce histidine-tagged (His-tagged) proteins containing the wild-type and Opdc Pax2 paired domains, recombinant plasmids were made in two steps. The 3′ end of the paired domain coding sequence was amplified by PCR from adult *Opdc* heterozygous kidney cDNA using primers 5′-GATA TGCACTGCAAAGCAGACC-3′ and 5′-GCGGATCCGGA TGATCCTGTTGATG-3′, which introduce a *Bam*HI site at the 3′ end. This was digested with *Nco*I and *Bam*HI, cloned into the *Nco*I and *Bam*HI sites of pET6H (51) and the resulting plasmid pET6HPax2NB verified by sequencing. The 5′ end of the Pax2 coding sequence was amplified by PCR from adult *Opdc* heterozygous kidney cDNA using primer pairs 5′-CCTCTGCCTCCCCATGGAT-3′ and 5′-CTTGATGCTG

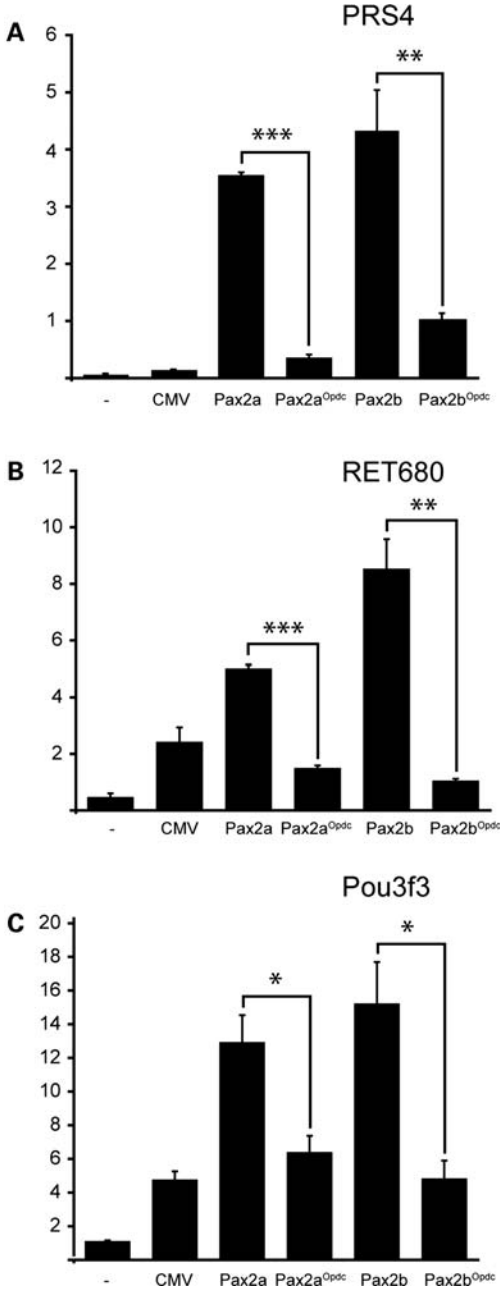

Figure 5. The *Opdc* mutation impairs Pax2 function. Mouse NIH 3T3 fibroblast cells were transiently transfected with (**A**) 400 ng of the plasmid PRS4Luc that contain five copies of the PRS4 binding site upstream of a luciferase reporter, (**B**) 400 ng of pGL3-Ret680 that contains a 680 bp fragment of the c-RET promoter sequence driving a luciferase reporter (25) and (**C**) 400 ng of pGL3-Pou3f3prom that contains a 3.2 kb *Bgl*II–*Not*I fragment from the *Pou3f3* gene promoter upstream of a luciferase reporter. For each, either no vector (−) or 400 ng of the following was co-transfected: CMV vector (CMV), CMV-Pax2a (Pax2a), CMV-Pax2a^{Opdc} (Pax2a^{Opdc}), CMV-Pax2b (Pax2b) or CMV-Pax2b^{Opdc} (Pax2a^{Opdc}). Each experiment was performed in triplicate, and mean firefly luciferase expression normalized to control renilla luciferase expression is shown + standard error. For each reporter, both Pax2a and Pax2b elicit robust induction of luciferase expression that is significantly reduced by the *Opdc* mutation (*t*-test; $^{*}P < 0.05$, $^{**}P \leq 0.01$, $^{***}P < 0.0001$). It is important to note that the activation of expression relative to that seen with the CMV by the Pax2 construct is the greatest with the PRS4 reporter shown in (A). For the RET680 and Pou3f3 reporter constructs shown in (B) and (C), there is some activation observed with the CMV construct and the relative increase in expression is much less when the wild-type CMV-Pax2 constructs were used.

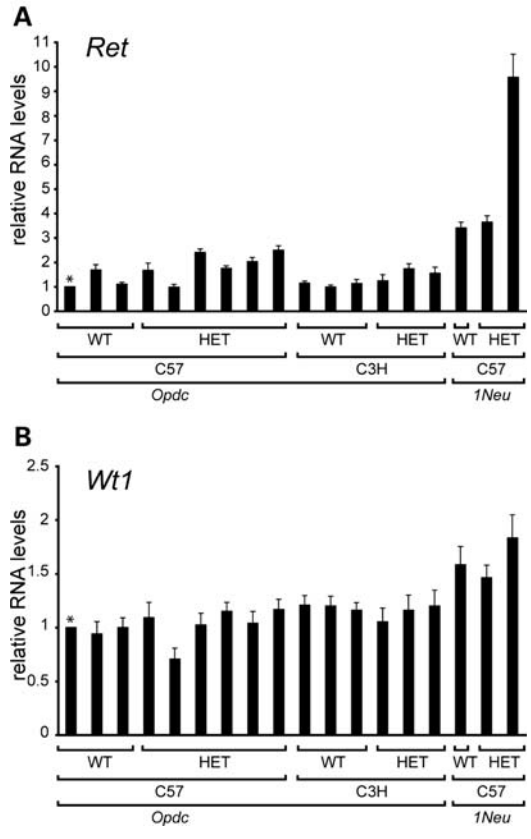

Figure 6. *Ret* and *Wt1* transcription levels are not significantly reduced in *Opdc*/+ and *1Neu*/+ E18.5 kidneys. *Ret* (**A**) and *Wt1* (**B**) RNA levels from wild-type and *Opdc*/+ E18.5 embryo littermates on the C57BL/6 and C3H backgrounds and wild-type and *1Neu*/+ E18.5 littermates on the C57BL/6 background. Mean values and standard deviations of three independent quantitative RT–PCR reactions are shown. The expression level of one wild-type sample from the *Opdc* line was designated as a calibrator and set to one (indicted by an asterisk) and the relative expression of other samples to this is shown.

CCAGTCTCGT-3′ that introduce an *Nco*I site adjacent to the start codon. This was digested with *Nco*I and cloned into the *Nco*I site of pET6HPax2NB. By restriction digest mapping and sequencing clones were identified, which contained either the wild-type (pET6HWTPD) or *Opdc* (pET6HOpdcPD) Pax2 sequence encoding amino acids 1–139 fused downstream of a 6× His tag encoded by the vector. Recombinant proteins were expressed in the *Escherichia coli* strain BL21 (DE3) pLysS essentially as described (52) and purified using Ni-NTA Agarose (Qiagen, Crawley, West Sussex, UK) following standard protocols. Purified proteins were analysed by sodium dodecyl sulphate–polyacrylamide gel electrophoresis to assess yield and purity and equal amounts of wild-type and mutant proteins were used in bandshift experiments.

Bandshift analysis

Probe sequences are shown in Figure 4E. For each DNA probe tested, double-stranded oligonucleotides with three or four base 5′ single-stranded extensions were either end-labelled by filling in the overhangs using radiolabelled nucleotides

and Klenow polymerase (Pax2Con, e5, P2, P6 and Enh) or DIG-labelled using terminal transferase and DIG-11-dUTP, following the manufacturer's instructions (Promega) (Dd and Pc). Bandshift analysis was carried out essentially as described (26). His-tagged paired domain proteins were incubated in 30 μl reactions on ice containing 10 mM HEPES (pH 7.9), 30 mM KCl, 20% glycerol, 1 mM EDTA, 1 mM β-mercaptoethanol, 250 μg/ml poly(dI.dC), 2.5 mg/ml bovine serum albumin and either 10 000–16 000 cpm (8×10^7–1.5×0^8 cpm/μg) radiolabelled DNA probe or 30 fmol DIG-labelled DNA probe for 30 min. Protein–DNA complexes were resolved by electrophoresing on pre-cooled 6% polyacrylamide gels in 0.5 × Tris-borate-EDTA buffer for 90 min at 240 V at 4°C. If using radiolabelled probes, the gels were dried onto DE81 paper (Whatman, GE Healthcare Life Sciences, Little Chalfont, Buckinghamshire, UK) and subjected to autoradiography. If using DIG-labelled probes, the gels were transferred to Hybond-N+ (GE Healthcare Life Sciences), processed according to manufacturer's protocol (Promega) and then subjected to autoradiography.

Magnetic resonance imaging

Pregnant mice were sacrificed by cervical dislocation at E14.5 or E15.5. Embryos were dissected and fixed for 7 days in 4% paraformaldehyde and 2 mM Gd-DTPA (Magnevist, Schering) in phosphate-buffered saline (PBS) at 4°C. Multi-embryo MRI was performed as described earlier (53) and the image files analysed using Amira software (TGS Europe, Merignas, France). For the 3D reconstruction of the inner ear, 3D visualization software was used to view the image data stacks. Manual segmentation and orthoslice tools were used to correct voxel size, view in transverse section, crop the data area and then paint the endolymphatic-filled membranous spaces of the cochlea and semi-circular canals.

Real-time quantitative RT–PCR

RNA was extracted from E18.5 kidneys using the RNeasy kit (Qiagen), and first strand cDNA was prepared using oligo-p$(dT)_{15}$ primers and the 1st Strand cDNA Synthesis Kit for RT–PCR (AMV) (Roche Diagnostics) using standard conditions. Quantitative RT–PCR analysis was performed using a Lightcycler® 480 Instrument (Roche Diagnostics Ltd, Burgess Hill, West Sussex, UK), following the manufacturer's instructions; 10 μl reactions containing 2 μl 10^{-1} dilution of cDNA, 5 μl 2× Lightcycler 480 Probes Master (Roche Diagnostics Ltd), 0.1 μM UPL probe and 0.5 μM of each primer were done in 384-well white plates. Assays were designed using the Probefinder software available at the Universal ProbeLibrary Assay Design Centre (http://qpcr.probefinder.com/roche3.html date last accessed 26/10/2010) (Roche Diagnostics Ltd); information about the primers and UPL probes used is available upon request. Reactions were incubated at 95°C for 10 min, then 55 cycles of 95°C for 10 s, 60°C for 30 s followed by a final incubation at 40°C for 30 s. Serial dilutions of wild-type cDNA were used to generate standard curves of each gene tested. Each assay was done in triplicate, and *Ret* and *Wt1* levels were quantified and normalized against *Pgk1* levels using the second derivative maximum method using the advanced relative quantification module of the Lightcycler® 480 software release 1.5.0. Essentially the same result was obtained using *Gapdh* as the reference gene. Both *Pgk1* and *Gapdh* have been validated as suitable reference genes for quantitative RT–PCR analysis of renal gene expression (54).

Embryo histology

After dissection, embryos were photographed and fixed overnight in 4% paraformaldehyde in PBS at 4°C. A small part of the tail was used for genotyping. After washing in PBS, they were dehydrated by immersion in a series of increasing concentrations of alcohol, embedded in paraffin wax, sectioned and stained with haematoxylin and eosin. Slides were viewed on a Leica MZFLIII fluorescence stereo microscope fitted with a Coolsnap colour camera (Roper Scientific, Tucson, AZ, USA). Image capture was controlled by in-house scripting of IPLab Spectrum (Scanalytics, Fairfax, VA, USA).

Statistical analysis

Values were expressed as mean ± standard deviation. A two-tailed unpaired Student's *t*-test was used for statistical analysis; $P < 0.05$ was considered significant.

ACKNOWLEDGEMENTS

We thank Malcolm Walkinshaw and David Fitzpatrick for useful discussions, Paul Perry for help with microscopy and Craig Nicol for help with figure preparation. We thank Peter Gruss, Gregory Dressler, Dirk-Jan Kleinjan and Patrick Brophy for constructs.

Conflict of Interest statement. The authors declare that they have no conflicting interests.

FUNDING

This work was supported by the Medical Research Council UK; The European Commission (EUMORPHIA project funded by FP5 grant no. QLG2-CT-2002-00930); the Wellcome Trust and the British Heart Foundation. The original ENU mutagenesis program was supported by funding from GlaxoSmithKline. Funding to pay the Open Access publication charges for this article was provided by the Medical Research Council.

REFERENCES

1. Schimmenti, L.A., Pierpont, M.E., Carpenter, B.L., Kashtan, C.E., Johnson, M.R. and Dobyns, W.B. (1995) Autosomal dominant optic nerve colobomas, vesicoureteral reflux, and renal anomalies. *Am. J. Med. Genet.*, **59**, 204–208.
2. Sanyanusin, P., Schimmenti, L.A., McNoe, L.A., Ward, T.A., Pierpont, M.E., Sullivan, M.J., Dobyns, W.B. and Eccles, M.R. (1995) Mutation of the PAX2 gene in a family with optic nerve colobomas, renal anomalies and vesicoureteral reflux. *Nat. Genet.*, **9**, 358–364.
3. Schimmenti, L.A., Cunliffe, H.E., McNoe, L.A., Ward, T.A., French, M.C., Shim, H.H., Zhang, Y.H., Proesmans, W., Leys, A., Byerly, K.A. *et al.* (1997)

Further delineation of renal-coloboma syndrome in patients with extreme variability of phenotype and identical PAX2 mutations. *Am. J. Hum. Genet.*, **60**, 869–878.
4. Tellier, A.-L., Amiel, J., Salomon, R., Jolly, D., Delezoide, A.-L., Auge, J., Gubler, M.-C., Munnich, A., Lyonnet, S., Antignac, C. *et al.* (1998) PAX2 expression during early human development and its mutations in renal hypoplasia with or without coloboma. *Am. J. Hum. Genet.*, **63**, A7.
5. Schimmenti, L.A., Shim, H.H., Wirtschafter, J.D., Panzarino, V.A., Kashtan, C.E., Kirkpatrick, S.J., Wargowski, D.S., France, T.D., Michel, E. and Dobyns, W.B. (1999) Homonucleotide expansion and contraction mutations of PAX2 and inclusion of Chiari 1 malformation as part of renal-coloboma syndrome. *Hum. Mutat.*, **14**, 369–376.
6. Bopp, D., Burri, M., Baumgartner, S., Frigerio, G. and Noll, M. (1986) Conservation of a large protein domain in the segmentation gene paired and in functionally related genes of *Drosophila*. *Cell*, **47**, 1033–1040.
7. Walther, C., Guenet, J.L., Simon, D., Deutsch, U., Jostes, B., Goulding, M.D., Plachov, D., Balling, R. and Gruss, P. (1991) Pax: a murine multigene family of paired box-containing genes. *Genomics*, **11**, 424–434.
8. Czerny, T., Schaffner, G. and Busslinger, M. (1993) DNA sequence recognition by Pax proteins: bipartite structure of the paired domain and its binding site. *Genes Dev.*, **7**, 2048–2061.
9. Xu, W., Rould, M.A., Jun, S., Desplan, C. and Pabo, C.O. (1995) Crystal structure of a paired domain-DNA complex at 2.5 A resolution reveals structural basis for Pax developmental mutations. *Cell*, **80**, 639–650.
10. Epstein, J.A., Glaser, T., Cai, J., Jepeal, L., Walton, D.S. and Maas, R.L. (1994) Two independent and interactive DNA-binding subdomains of the Pax6 paired domain are regulated by alternative splicing. *Genes Dev.*, **8**, 2022–2034.
11. Xu, H.E., Rould, M.A., Xu, W., Epstein, J.A., Maas, R.L. and Pabo, C.O. (1999) Crystal structure of the human Pax6 paired domain–DNA complex reveals specific roles for the linker region and carboxy-terminal subdomain in DNA binding. *Genes Dev.*, **13**, 1263–1275.
12. Eccles, M.R. and Schimmenti, L.A. (1999) Renal-coloboma syndrome: a multi-system developmental disorder caused by PAX2 mutations. *Clin. Genet.*, **56**, 1–9.
13. Devriendt, K., Matthijs, G., Van Damme, B., Van Caesbroeck, D., Eccles, M., Vanrenterghem, Y., Fryns, J.P. and Leys, A. (1998) Missense mutation and hexanucleotide duplication in the PAX2 gene in two unrelated families with renal-coloboma syndrome (MIM 120330). *Hum. Genet.*, **103**, 149–153.
14. Higashide, T., Wada, T., Sakurai, M., Yokoyama, H. and Sugiyama, K. (2005) Macular abnormalities and optic disk anomaly associated with a new PAX2 missense mutation. *Am. J. Ophthalmol.*, **139**, 203–205.
15. Favor, J., Sandulache, R., Neuhauser-Klaus, A., Pretsch, W., Chatterjee, B., Senft, E., Wurst, W., Blanquet, V., Grimes, P., Sporle, R. and Schughart, K. (1996) The mouse Pax2(1Neu) mutation is identical to a human PAX2 mutation in a family with renal-coloboma syndrome and results in developmental defects of the brain, ear, eye, and kidney. *Proc. Natl Acad. Sci. USA*, **93**, 13870–13875.
16. Sanyanusin, P., McNoe, L.A., Sullivan, M.J., Weaver, R.G. and Eccles, M.R. (1995) Mutation of PAX2 in two siblings with renal-coloboma syndrome. *Hum. Mol. Genet.*, **4**, 2183–2184.
17. Alur, R.P., Vijayasarathy, C., Brown, J.D., Mehtani, M., Onojafe, I.F., Sergeev, Y.V., Boobalan, E., Jones, M., Tang, K., Liu, H. *et al.* (2010) Papillorenal syndrome-causing missense mutations in PAX2/Pax2 result in hypomorphic alleles in mouse and human. *PLoS Genet.*, **6**, e1000870.
18. Torres, M., Gomez-Pardo, E., Dressler, G.R. and Gruss, P. (1995) Pax-2 controls multiple steps of urogenital development. *Development*, **121**, 4057–4065.
19. Torres, M., Gomez-Pardo, E. and Gruss, P. (1996) Pax2 contributes to inner ear patterning and optic nerve trajectory. *Development*, **122**, 3381–3391.
20. Schwarz, M., Alvarez-Bolado, G., Urbanek, P., Busslinger, M. and Gruss, P. (1997) Conserved biological function between Pax-2 and Pax-5 in midbrain and cerebellum development: evidence from targeted mutations. *Proc .Natl Acad. Sci. USA*, **94**, 14518–14523.
21. Thaung, C., West, K., Clark, B.J., McKie, L., Morgan, J.E., Arnold, K., Nolan, P.M., Peters, J., Hunter, A.J., Brown, S.D.M. *et al.* (2002) Novel ENU-induced eye mutations in the mouse: models for human eye disease. *Hum. Mol. Genet.*, **11**, 755–767.
22. Garvie, C.W., Hagman, J. and Wolberger, C. (2001) Structural studies of Ets-1/Pax5 complex formation on DNA. *Mol. Cell*, **8**, 1267–1276.
23. Discenza, M.T., He, S., Lee, T.H., Chu, L.L., Bolon, B., Goodyer, P., Eccles, M. and Pelletier, J. (2003) WT1 is a modifier of the Pax2 mutant phenotype: cooperation and interaction between WT1 and Pax2. *Oncogene*, **22**, 8145–8155.
24. Porteous, S., Torban, E., Cho, N.P., Cunliffe, H., Chua, L., McNoe, L., Ward, T., Souza, C., Gus, P., Giugliani, R. *et al.* (2000) Primary renal hypoplasia in humans and mice with PAX2 mutations: evidence of increased apoptosis in fetal kidneys of Pax2(1Neu) ± mutant mice. *Hum. Mol. Genet.*, **9**, 1–11.
25. Clarke, J.C., Patel, S.R., Raymond, R.M., Jr, Andrew, S., Robinson, B.G., Dressler, G.R. and Brophy, P.D. (2006) Regulation of c-Ret in the developing kidney is responsive to Pax2 gene dosage. *Hum. Mol. Genet.*, **15**, 3420–3428.
26. Epstein, J., Cai, J., Glaser, T., Jepeal, L. and Maas, R. (1994) Identification of a Pax paired domain recognition sequence and evidence for DNA-dependent conformational changes. *J. Biol. Chem.*, **269**, 8355–8361.
27. Hoey, T. and Levine, M. (1988) Divergent homeo box proteins recognize similar DNA sequences in *Drosophila*. *Nature*, **332**, 858–861.
28. Schwarz, M., Cecconi, F., Bernier, G., Andrejewski, N., Kammandel, B., Wagner, M. and Gruss, P. (2000) Spatial specification of mammalian eye territories by reciprocal transcriptional repression of Pax2 and Pax6. *Development*, **127**, 4325–4334.
29. Bouchard, M., Grote, D., Craven, S.E., Sun, Q., Steinlein, P. and Busslinger, M. (2005) Identification of Pax2-regulated genes by expression profiling of the mid-hindbrain organizer region. *Development*, **132**, 2633–2643.
30. Dressler, G.R. and Douglass, E.C. (1992) Pax-2 is a DNA-binding protein expressed in embryonic kidney and Wilms tumor. *Proc. Natl Acad. Sci. USA*, **89**, 1179–1183.
31. Dressler, G.R., Wilkinson, J.E., Rothenpieler, U.W., Patterson, L.T., Williams-Simons, L. and Westphal, H. (1993) Deregulation of Pax-2 expression in transgenic mice generates severe kidney abnormalities. *Nature*, **362**, 65–67.
32. Fickenscher, H.R., Chalepakis, G. and Gruss, P. (1993) Murine Pax-2 protein is a sequence-specific trans-activator with expression in the genital system. *DNA Cell Biol.*, **12**, 381–391.
33. Keller, S.A., Jones, J.M., Boyle, A., Barrow, L.L., Killen, P.D., Green, D.G., Kapousta, N.V., Hitchcock, P.F., Swank, R.T. and Meisler, M.H. (1994) Kidney and retinal defects (Krd), a transgene-induced mutation with a deletion of mouse chromosome 19 that includes the Pax2 locus. *Genomics*, **23**, 309–320.
34. Kozmik, Z., Czerny, T. and Busslinger, M. (1997) Alternatively spliced insertions in the paired domain restrict the DNA sequence specificity of Pax6 and Pax8. *EMBO J.*, **16**, 6793–6803.
35. Hanson, I. and Van Heyningen, V. (1995) Pax6: more than meets the eye. *Trends Genet.*, **11**, 268–272.
36. Hanson, I.M., Fletcher, J.M., Jordan, T., Brown, A., Taylor, D., Adams, R.J., Punnett, H.H. and Van Heyningen, V. (1994) Mutations at the PAX6 locus are found in heterogeneous anterior segment malformations including Peters' anomaly. *Nat. Genet.*, **6**, 168–173.
37. Tang, H.K., Chao, L.Y. and Saunders, G.F. (1997) Functional analysis of paired box missense mutations in the PAX6 gene. *Hum. Mol. Genet.*, **6**, 381–386.
38. Hanson, I., Churchill, A., Love, J., Axton, R., Moore, T., Clarke, M., Meire, F. and Van Heyningen, V. (1999) Missense mutations in the most ancient residues of the PAX6 paired domain underlie a spectrum of human congenital eye malformations. *Hum. Mol. Genet.*, **8**, 165–172.
39. Gronskov, K., Rosenberg, T., Sand, A. and Brondum-Nielsen, K. (1999) Mutational analysis of PAX6: 16 novel mutations including 5 missense mutations with a mild aniridia phenotype. *Eur. J. Hum. Genet.*, **7**, 274–286.
40. Azuma, N., Hotta, Y., Tanaka, H. and Yamada, M. (1998) Missense mutations in the PAX6 gene in aniridia. *Invest. Ophthalmol. Vis. Sci.*, **39**, 2524–2528.
41. Taranta, A., Palma, A., De, L., Romanzo, A., Massella, L., Emma, F. and Dello Strologo, L. (2007) Renal-coloboma syndrome: a single nucleotide deletion in the PAX2 gene at exon 8 is associated with a highly variable phenotype. *Clin. Nephrol.*, **67**, 1–4.
42. Nishimoto, K., Iijima, K., Shirakawa, T., Kitagawa, K., Satomura, K., Nakamura, H. and Yoshikawa, N. (2001) PAX2 gene mutation in a family with isolated renal hypoplasia. *J. Am. Soc. Nephrol.*, **12**, 1769–1772.
43. Sellick, G.S., Longman, C., Tolmie, J., Newbury-Ecob, R., Geenhalgh, L., Hughes, S., Whiteford, M., Garrett, C. and Houlston, R.S. (2004)

Genomewide linkage searches for Mendelian disease loci can be efficiently conducted using high-density SNP genotyping arrays. *Nucleic Acids Res.*, **32**, e164.
44. Winston, J.B., Erlich, J.M., Green, C.A., Aluko, A., Kaiser, K.A., Takematsu, M., Barlow, R.S., Sureka, A.O., LaPage, M.J., Janss, L.L. and Jay, P.Y. (2010) Heterogeneity of genetic modifiers ensures normal cardiac development. *Circulation*, **121**, 1313–1321.
45. Guay-Woodford, L.M. (2003) Murine models of polycystic kidney disease: molecular and therapeutic insights. *Am. J. Physiol. Renal. Physiol.*, **285**, F1034–F1049.
46. Matteson, P.G., Desai, J., Korstanje, R., Lazar, G., Borsuk, T.E., Rollins, J., Kadambi, S., Joseph, J., Rahman, T., Wink, J. *et al.* (2008) The orphan G protein-coupled receptor, Gpr161, encodes the vacuolated lens locus and controls neurulation and lens development. *Proc. Natl Acad. Sci. USA*, **105**, 2088–2093.
47. Churchill, G.A., Airey, D.C., Allayee, H., Angel, J.M., Attie, A.D., Beatty, J., Beavis, W.D., Belknap, J.K., Bennett, B., Berrettini, W. *et al.* (2004) The Collaborative Cross, a community resource for the genetic analysis of complex traits. *Nat. Genet.*, **36**, 1133–1137.
48. Cunliffe, H.E., McNoe, L.A., Ward, T.A., Devriendt, K., Brunner, H.G. and Eccles, M.R. (1998) The prevalence of PAX2 mutations in patients with isolated colobomas or colobomas associated with urogenital anomalies. *J. Med. Genet.*, **35**, 806–812.
49. Baumer, N., Marquardt, T., Stoykova, A., Spieler, D., Treichel, D., Ashery-Padan, R. and Gruss, P. (2003) Retinal pigmented epithelium determination requires the redundant activities of Pax2 and Pax6. *Development*, **130**, 2903–2915.
50. Czerny, T. and Busslinger, M. (1995) DNA-binding and transactivation properties of Pax-6: three amino acids in the paired domain are responsible for the different sequence recognition of Pax-6 and BSAP (Pax-5). *Mol. Cell Biol.*, **15**, 2858–2871.
51. Hu, C.H., McStay, B., Jeong, S.W. and Reeder, R.H. (1994) xUBF, an RNA polymerase I transcription factor, binds crossover DNA with low sequence specificity. *Mol. Cell Biol.*, **14**, 2871–2882.
52. Studier, F.W., Rosenberg, A.H., Dunn, J.J. and Dubendorff, J.W. (1990) Use of T7 RNA polymerase to direct expression of cloned genes. *Methods Enzymol.*, **185**, 60–89.
53. Schneider, J.E., Bose, J., Bamforth, S.D., Gruber, A.D., Broadbent, C., Clarke, K., Neubauer, S., Lengeling, A. and Bhattacharya, S. (2004) Identification of cardiac malformations in mice lacking Ptdsr using a novel high-throughput magnetic resonance imaging technique. *BMC Dev. Biol.*, **4**, 16.
54. Cui, X., Zhou, J., Qiu, J., Johnson, M.R. and Mrug, M. (2009) Validation of endogenous internal real-time PCR controls in renal tissues. *Am. J. Nephrol.*, **30**, 413–417.
55. Humphrey, W., Dalke, A. and Schulten, K. (1996) VMD: visual molecular dynamics. *J. Mol. Graphics*, **14**, 33–38.